A Combined Topology Formation and Rate Allocation Algorithm for Aeronautical Ad Hoc Networks

Vasileios Megas, Sandra Hoppe, Mustafa Ozger, Dominic Schupke, and Cicek Cavdar

Abstract—This paper addresses the problem of providing internet connectivity to aircraft flying above the ocean without using satellite connectivity given the lack of ground network infrastructure in the relevant oceanic areas. Is it possible to guarantee a minimum flow rate to each aircraft flying over an ocean by forming an aeronautical ad hoc network and connecting that network to internet via a set of limited number of ground base stations at the coast as anchor points? We formulated the problem as mixed-integer-linear programming (MILP) to maximize the number of aircraft with flow data rate above a certain threshold. Since this multi-commodity flow problem is at least NP-complete, we propose a two-phase heuristic algorithm to efficiently form topology and assign flows to each aircraft by maximizing the minimum flow. The performance of the heuristic algorithm is evaluated over the North Atlantic Corridor, heuristic performs only 8% less than the optimal result with low densities. In high network densities, the connectivity percentage changes from 70% to 40% under 75 Mbps data rate threshold. Furthermore, the connectivity percentage is investigated for different network parameters such as altitude and compared to upper and lower bounds and a baseline algorithm.

Index Terms—Topology formation, rate allocation, aerial networks, ad-hoc networks, direct air to ground communication, air to air communication, mixed integer linear programming, aircraft connectivity

1 Introduction

PROVIDING broadband Internet connectivity to terrestrial users has been one of the main struggles for fifth generation (5G) wireless networks and beyond [2]. On the other hand, onboard cellular connectivity for aircraft passengers has been one of the venues that remain without high data rate communications. According to International Air Transport Association (IATA) forecasts, the number of aircraft passengers will reach 8.2 billion by 2037 with a 3.5% compound annual growth rate [3]. Although this forecast is from 2018, we expect this number to occur a few years later. In addition to the increase in the aircraft passengers, they will be more demanding to have in-flight connectivity. Hence, this behavior indicates an ever-increasing demand for high data rate connectivity in the sky and related services.

Next Generation Mobile Networks (NGMN) states that three-dimensional connectivity of aircraft is vital for civil aviation and passenger services [4]. Key performance indicators (KPIs) are defined to be 1.2 Gbps and 0.6 Gbps per aircraft for downlink and uplink communications, respectively [4]. Achieving these targets on KPIs is an ambitious goal albeit with some developments in aerial communications.

Satellite Communication (SC) and direct air to ground communication (DA2GC) are the two options to provide backhaul capacity for in-flight connectivity [5]. Current aircraft connectivity depends on mostly geostationary Earth orbit (GEO) satellites, which are deployed at 35786 km away from the Earth. The main disadvantages of the GEO satellite connectivity are high delays with at least 280 milliseconds (ms) round trip time, and limited data rate due to sharing the existing GEO satellite capacity with a high number of users within their large coverage areas [6], [7]. Other alternatives for satellite connectivity are medium Earth orbit (MEO) and low Earth orbit (LEO) satellites deployed at a minimum altitude of 600 km above the Earth surface [8]. MEO and LEO satellites provide connectivity with a lower delay and higher throughput than GEO satellites. One main drawback of the MEO and LEO satellites is that they have smaller footprints than those of GEO satellites. Hence, mega-constellations satellite networks are needed [9]. Recently, companies such as SpaceX, OneWeb, and Facebook are deploying LEO satellite networks to provide global Internet coverage for all people [10]. Although LEO satellites are promising, some challenges still exist in terms of cost and scale for their deployment to cover the Earth. Furthermore, it is not clear to utilize these constellations for the connectivity of aircraft passengers.

Another alternative for providing backhaul connectivity to aircraft is DA2GC. Base stations (BSs) are deployed and

- *Vasileios Megas, Mustafa Ozger, and Cicek Cavdar are with the School of Electrical Engineering and Computer Science, KTH Royal Institute of Technology, 114 28 Stockholm, Sweden. E-mail: {vmegas, ozger, cavdar}@kth.se.*
- *Sandra Hoppe was with the Airbus, 85521 Ottobrunn/Munich, Germany. He is now with the Nokia Strategy & Technology, 81541 Munich, Germany. E-mail: sandra.hoppe@nokia-bell-labs.com.*
- *Dominic Schupke is with the Airbus, Central Research and Technology, Communication Technologies, 85521 Ottobrunn/Munich, Germany. E-mail: dominic.schupke@airbus.com.*

Manuscript received 19 May 2021; revised 18 August 2022; accepted 14 October 2022. Date of publication 0 2022; date of current version 0 2022.
This work was partially funded by EU Celtic Next Project, 6G for Connected Sky (6G-SKY) with the support of Vinnova, Swedish Innovation Agency.
(Corresponding author: Mustafa Ozger.)
Digital Object Identifier no. 10.1109/TMC.2022.3217924

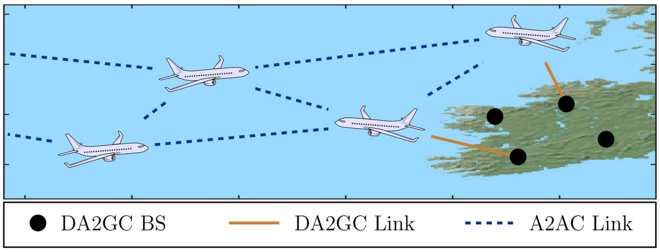

Fig. 1. Extending coverage of DA2GC networks with A2AC links.

dedicated for air to ground (A2G) communication [1], [11]. Their antennas are tilted upwards to serve the aircraft over the mainland. DA2GC has a lower delay of around 5-10 ms and higher data rates than GEO satellites [1]. One of the main drawbacks of DA2GC is that its coverage is limited to the ground deployment of DA2GC BSs. Hence, the DA2GC coverage is over continental areas with areas close to the shoreline.

Commercial DA2GC solutions are offered today, however they do not achieve the NGMN KPI targets. For instance, Gogo Inc. provides a data rate up to 9.8 Mbps when operating at 800 MHz carrier frequency in the USA and Canada [12]. More recent Gogo solution boosts the capacity by multi-carrier Long Term Evolution (LTE) signals for higher bandwidth [13]. Gogo Inc. also focuses on building a 5G network on top of their existing infrastructure with the use of 2.4 GHz bands for DA2GC and advanced beamforming technology [14]. Furthermore, SmartSky provides inflight connectivity for business jets via their 4G-LTE based networks [15]. The European Aviation Network (EAN) also provides connectivity for commercial aircraft with a solution that integrates satellite and A2G communications [16]. It provides a data rate of up to 75 Mbps per aircraft over the European continent with a 40 ms delay and a communication range of 150 km from an EAN BS. Despite the developments in DA2GC technology, the goal of 1.2 Gbps for downlink has not been achieved yet.

Without relying on SC, only DA2GC does not provide a global coverage since 2/3 of the Earth surface is covered by water. Air to air communication (A2AC) is a natural way to overcome this limitation by extending the coverage of DA2GC networks. Fig. 1 shows the extension of the DA2GC connectivity by utilizing A2AC link between the aircraft. Hence, aircraft in the middle of the ocean can have a certain degree of connectivity via A2AC links.

A2AC has been studied to extend coverage in different segments of airspace. For instance, A2AC is proposed for relaying data and providing coverage to the areas without infrastructure by using unmanned aerial vehicles (UAVs) in very low-level airspace [17]. On the other hand, commercial aircraft having DA2GC connectivity can use A2AC links to extend the coverage beyond the mainland toward the oceans in [1], [5].

From a networking point of view, the extension of DA2GC via A2AC establishes multi-hop wireless ad hoc networks with flying vehicles such as UAVs and commercial aircraft. They can comprise of only UAVs as in [18], [19] or only commercial aircraft as in [1], [20], [21], [22] or a mix of them as in [23], [24], [25]. Different terms such as flying ad hoc networks (FANETs) [19] and airborne Internet [22] are used in literature for these types of aerial networks without infrastructure. Since the main focus in this paper is aircraft flying at higher altitudes, we adopt the term "Aeronautical Ad Hoc Networks (AANETs)"[1].

In this article, AANETs exhibit spatio-temporal dynamics due to the movement of the aircraft and their antenna characteristics, the maximum number of nodes that each aircraft node can communicate (i.e., nodal degree), aircraft traffic, their signal to interference plus noise ratio (SINR) levels, and backhaul capacity from DA2GC. According to these dynamics, the topology of the AANETs must be decided, and data rates for the established A2AC links must be allocated by jointly solving a flow assignment problem to satisfy quality of service (QoS) requirements for each aircraft depending on the connectivity service applications. In this paper, we first formulate a combined topology formation and rate allocation problem subject to the network-specific and aircraft-specific constraints as a mixed integer linear program (MILP). "Rate allocation" is defined as a specific case of a flow assignment problem, where aircraft are nodes both acting as sink nodes and pass-through nodes. The ultimate objective of the formulated problem is to maximize the number of aircraft having a data rate higher than a threshold. This problem has been studied in [1] for a small number of aircraft in AANETs, i.e., for up to 60 aircraft nodes over the North Atlantic Corridor. However, due to the nature of MILP, computations to obtain the optimal solutions become prohibitive with the increasing number of aircraft in the network. Hence, the main contribution of this paper is to propose a combined topology formation and rate allocation algorithm that can scale for larger networks. The proposed algorithm is near-optimal when it is compared to the solution from MILP for a low density of aircraft in AANETs over the North Atlantic Corridor. We study the performance for all possible aircraft densities based on real aircraft traces and network and aircraft parameters. Hence, our contributions in this paper are itemized as follows:

- We formulate a combined topology formation and rate allocation problem in AANETs considering antenna characteristics, the maximum number of nodes that each aircraft node can communicate, aircraft traffic, SINR levels of A2AC links, aircraft altitude and backhaul capacity from the DA2GC links used as anchor to connect the Internet.
- We use parameters with realistic settings, i.e., nodal degree, directional antennas, and use data sets on commercial flights over the North Atlantic Corridor from FlightRadar24 [26] to aim at accurate results with a consideration of interference due to topology formation.
- We propose an efficient algorithm, which can scale for larger networks, to determine network topology and allocation of rates.
- We perform extensive simulations to study the performance of the proposed algorithm and compare its performance with an upper bound, a lower bound a baseline algorithm, and the optimal solution.

1. Hereafter, AANETs refer to the mobile ad hoc networks consisting of only commercial aircraft.

The paper is organized as follows. Section 2 provides related work and the contribution of the paper. Section 3 explains the system model for AANETs over a geographical area without terrestrial infrastructure such as oceans to provide Internet connectivity. Section 4 explains the mathematical formulation of the combined topology formation and rate allocation problem as a MILP. Section 5 describes the proposed heuristic algorithm for topology formation and rate allocation. Section 6 explains the performance of the proposed algorithm via simulations in a specific region, i.e., the North Atlantic Corridor. Finally, Section 7 concludes our paper.

2 Related Work

DA2GC is a key technology to provide backhaul connectivity to the sky. Hence, in addition to the commercial activities by companies such as EAN and Gogo, studies to enable high capacity air to ground links have been conducted. For instance, [27], [28] utilize 1000 antenna elements and multi-user beamforming to achieve the theoretical 1.2 Gbps DA2GC data rate. Furthermore, to efficiently use the spectrum resources in the sky and boost the DA2GC capacity, the authors in [29] coordinate the beam selection and spectrum allocation.

In addition to the efforts to boost the DA2GC capacity, A2AC can overcome the challenge of DA2GC limited coverage. It results in the formation of AANETs over the regions without DA2GC coverage, such as oceans. The authors in [30] envision a future AANET with three key elements. They are high capacity optical communication links, hybrid radio frequency (RF)/optical communication networking between the elements in the sky such as high altitude platforms (HAPs) and aircraft, and backhaul connectivity via optical links from ground stations to the deployed HAPs. Although the proposed architecture is promising, the running cost of HAPs and limitations of optical links due to weather conditions are the two main obstacles. The authors in [20] propose a network architecture with commercial aircraft and ground gateway nodes, which are connected via free-space optical communications (FSOC). This network architecture has high capacity communications via highly directional FSOC links. However, those links can be unreliable in bad weather conditions, and FSOC imposes limitations on the nodal degree.

The authors in [5] investigate the integration of A2AC with SC and DA2GC only for two-hop communications to overcome the coverage problem without any consideration of networking between aircraft. Furthermore, [20] deals with topology management in AANETs. The ultimate goal is to manage the topology in AANETs with a large number of aircraft by deciding on the direction of the links and connections via candidate graph theory algorithms. However, the current graph theory algorithms such as minimum spanning tree exhibit inefficiencies due to the directional links and nodal degree constraints. They extend the existing algorithms by imposing degree constraints and avoiding tree-like structures. However, the proposed algorithms do not provide any performance guarantees and data rate considerations.

Other than network architectures for AANET with different technologies such as FSOC, forming an AANET over the North Atlantic Corridor has been an interest of research in literature. For instance, the link probability is calculated for the aircraft crossing the North Atlantic based on the real aircraft traces in [31]. Furthermore, the derived analytical model captures the traffic characteristics and neighbor distance distributions of aircraft over the North Atlantic Corridor. In [32], an aircraft mobility model is constructed over the North Atlantic Corridor by considering real aircraft traces from 2008 with the inclusion of probabilistic delays and cancellations for the flights. However, these studies do not consider the topology formation and satisfaction of QoS requirements from the aircraft passengers.

Other than the derivation of link probabilities and mobility models, many proposals for routing algorithms exist as well. The authors in [33] propose a routing algorithm for AANETs, which are airborne mesh networks formed by commercial aircraft having directional antennas over the North Atlantic Corridor. The proposed algorithm focuses on forwarding the packets according to the speed of the aircraft in the next hop and its buffer load. Furthermore, load balancing between the gateway nodes on the ground is performed via a handover strategy. [33] aims to ensure the all DA2GC links are fully utilized without any packet drop. [34] focuses on the problem of joint gateway allocation, routing, and scheduling in AANETs to minimize experienced average packet delay. Since the problem is non-convex, the authors in [34] divide the problem into two steps. The first step is the minimization of hop count with a scheduling constraint. The second step is the minimization of the packet delay. However, these routing solutions are implemented based on an assumed topology of AANETs without considering topology formation with physical communication and antenna constraints.

In [32], an optimal max-min fair network capacity allocation scheme is proposed. However, the system model in [1] utilizes omnidirectional antennas without any nodal degree constraint and does not consider interference by the transmission of neighboring aircraft in AANETs over the North Atlantic corridor. The topology formation and utilization of the link resources in AANETs have not been studied extensively with a focus on the challenges posed by AANETs. The research gap we focus on in this paper is the combined topology formation and rate allocation in AANETs with network parameters and realistic settings.

3 System Model

The system model consists of two parts. The first one is the communication model focusing on DA2GC backhaul links, A2AC links and SINR in AANETs. The second part is for modeling the network.

3.1 Communications Model

In Europe, the carrier frequencies of 1.9 GHz and 5.8 GHz are designated for DA2GC by European Telecommunications Standards Institute (ETSI) [35]. For our system model to comply with the standards, we adopted the designated frequency band between 5855 MHz and 5875 MHz by ETSI with a resulting bandwidth of 20 MHz for DA2GC links.

To the best of our knowledge, there is no designated frequency range for A2AC. Millimeter-Waves (mm-Waves) is one of the candidates for A2AC due to their high bandwidth. One drawback is the incurred high path losses due to their short wavelengths. On the other hand, it also enables smaller antenna dimensions and increasing the number of antenna elements to have higher gain to compensate for these path losses. In this paper, we adopt 31 GHz as the operating frequency for A2AC links. The reason for selecting this frequency band is its lower exposure to atmospheric attenuation than other mm-Waves frequency bands. The backhaul DA2GC link has 20 MHz bandwidth. Hence, we assume the same bandwidth for A2AC links.

DA2GC BSs are presumed to be deployed at hills or on the rooftops of high building such that the aircraft connecting to the DA2GC BS are in line of sight (LoS) condition. Furthermore, established A2AC links have LoS condition due to their cruising altitude and absence of obstacles. Consequently, LoS path is more dominant in comparison to non-LoS paths for both DA2GC and A2AC. Due to the dominant LoS path, these channels are modeled as Rician fading channels [25], [36]. The ratio between power of LoS component and total power of non-LoS components is called K-factor. It is calculated as

$$K = \frac{s^2}{2\sigma^2}, \tag{1}$$

where s^2 is the power of LoS component of the received signal, and $2\sigma^2$ is the total power of non-LoS components. Let X denote the random variable capturing the channel gain following Rician distribution, whose probability density function is given as

$$f_X(x) = \frac{x}{\sigma^2} exp\left(\frac{-(x^2+s^2)}{2\sigma^2}\right) I_0\left(\frac{xs}{\sigma^2}\right), \tag{2}$$

where $I_0(.)$ is the modified Bessel function of the first kind with order zero. Furthermore, to have a simple implementation, the mean received power is required to be unchanged, i.e., $E[|X|^2] = s^2 + 2\sigma^2 = 1$ [36].

Path loss (PL) for aerial communications is defined as

$$\xi(d) = \left(\frac{4\pi d f}{\omega}\right)^2, \tag{3}$$

where d is the distance between the two aircraft, f is the carrier frequency, and ω is the speed of light. Due to the curvature of the Earth, the physical communication distance is limited. Unless otherwise stated, for a cruising altitude of 10 km in our simulations, the maximum LoS distance (i.e., physical A2AC distance) is approximately 700 km. The physical communication distance limit for DA2GC is half of the limit for A2AC.

The thermal noise of the receiver is $N = kTB$, where k is the Boltzmann constant, T is the temperature in Kelvin (K), and B is the bandwidth in Hz. The temperature at aircraft cruising altitude is assumed to be $T = 223.25$ K [37]. It gives a noise figure of $N = -132.1009$ dBW. Hence, the received power at a communication distance of d meters is calculated as

$$P(d) = P_t + G_t + G_r - \xi(d) - N + |X^2| \quad [dB], \tag{4}$$

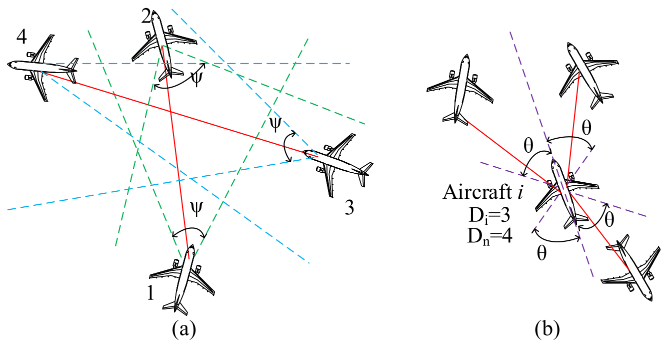

Fig. 2. (a) Interference caused by link $(3,4)$ to link $(1,2)$. The solid red lines show A2AC links, the dashed lines depict the beams of the aircraft antennas. (b) An example to illustrate connections of aircraft i and its nodal degree.

where P_t is the transmit power, and G_t and G_r the transmitter and receiver gains, respectively, and $|X^2|$ is the power gain due to the Rician fading channel. Transmit power is assumed to be 20 dBW [32]. Antenna gains at the receiver and transmitter sides are assumed to be $G_{t,A2AC} = G_{r,A2AC} =$ 32.2 dB for A2AC [1]. Antenna gain at BS ($G_{t,BS}$) and antenna gain at aircraft ($G_{r,DA2GC}$) are assumed to be 29.2 and 14.5 dB, respectively, for DA2GC [1].

The maximum number of connections of the aircraft depends on the number of antennas installed on the aircraft. Due to strict regulations and certifications for aircraft as well as weight/drag and physical challenges like cabling, the number of antennas has a limitation, which imposes a constraint on the nodal degree. We also assume that installed antennas have transmit and receive pairs to enable transmission and reception simultaneously. Nodal degree for an aircraft i is denoted by D_n, which is the maximum number of communication links for all aircraft as a network parameter. One should note that D_i for aircraft i is the number of connection links in a formed topology, which is less than or equal to D_n. Each antenna has a certain maximum turning angle with respect to the flight direction of the aircraft, which is denoted by the maximum antenna steering angle of θ. The receive and transmit antennas are placed at the front and back of the aircraft. In this model, we neglect the effect of shadowing by the aircraft structure as well as the exact placement of DA2GC and A2AC antennas. While these per-aircraft characteristics cannot be modeled in this paper, it needs to be taken into account when implementing the system as it might imply the need of more antennas or different antenna characteristics than in the ideal case.

Topology formation and rate allocation are also affected by the interference. If two aircraft reside within each other's beam, they cause interference to each other. Fig. 2a shows four aircraft with two A2AC links. The first A2AC link (1,2) is from aircraft 1 to aircraft 2. The second one (3,4) is from aircraft 3 to aircraft 4. Aircraft 2 receives interference from aircraft 3 due to its transmission towards aircraft 4. Beamwidth, which is denoted by ψ, is an important factor to determine the interference. As seen in Fig. 2a, the receive antenna beamwidth of aircraft 2 overlaps with the transmit antenna beamwidth of aircraft 3, which results in interference. Fig. 2b shows an example illustration of links in a formed topology with red lines. For this specific example,

TABLE 1
Data Rate for Different SINR Intervals [1], [38]

SINR	Modulation	Rate (Mbps)
$(-\infty, -9.478)$	Weak Signal	0
$[-9.478, -3)$	QPSK	4
$[-3, -0.2)$	QPSK	10
$[-0.2, 4.9)$	QPSK	22
$[4.9, 7)$	16-QAM	37
$[7, 8.8)$	16-QAM	48
$[8.8, 10.5)$	16-QAM	61
$[10.5, 13)$	64-QAM	69
$[13, 14.5)$	64-QAM	84
$[14.5, 16.2)$	64-QAM	98
$[16.2, 18.8)$	64-QAM	114
$[18.8, 20.5)$	64-QAM	129
$[20.5, 22)$	256-QAM	140
$[22, 23.7)$	256-QAM	157
$[23.7, 27.3)$	256-QAM	174
$[27.3, +\infty)$	256-QAM	187

let us assume the maximum number of links that aircraft can form is four, i.e., $D_n = 4$. However, aircraft i has only three A2AC links, i.e., $D_i = 3$. Fig. 2b also illustrates the maximum antenna steering angle θ for aircraft i, which is the maximum angle the aircraft i directs its antenna.

Interference between DA2GC links and A2AC links does not exist since they operate in different frequency bands. We assume that ground DA2GC BSs utilize beamforming and beamsteering technologies, which lead to narrow beams that do not interfere with each other. SINR for an A2AC link (i, j) from aircraft i to aircraft j can be calculated as follows:

$$SINR_{i,j} = \frac{P_{i,j}}{N_0 + \sum_{(k,l)\in E} I_{i,j}^{k,l} P_{k,j} z_{k,l}}, \tag{5}$$

where $P_{i,j}$ is the received power by aircraft j due to transmission by aircraft i, $I_{i,j}^{k,l}$ is an indicator function, which would be 1 if A2AC link from aircraft k to aircraft l causes interference to link (i, j), $z_{k,l}$ is a binary variable for the formed topology, which becomes 1 if the link between aircraft k and l is formed in the network, and N_0 is the noise power.

A dynamic modulation scheme is adopted to exploit SINR levels efficiently. Table 1 shows the relation between SINR levels and the used modulations with corresponding LTE data rates [1], [38]. For low SINR levels, quadrature phase shift keying (QPSK) modulation is utilized. For intermediate SINR ranges, 16-quadrature amplitude modulation (QAM) or 64-QAM are used depending on the SINR levels. 256-QAM is used for higher SINR levels. Higher modulations provide a higher data rate but require a higher SINR to avoid high bit error rate (BER). We assume LTE standards, however other radio access technologies can be also utilized as well instead. To calculate the bit rate, we consider a setting with 12 subcarriers, seven orthogonal frequency division multiple access (OFDMA) symbols, and two slots per ms [39]. For a bandwidth of 20 MHz, we can get up to 12.6 symbols/s when 256-QAM modulation is used. By considering a 2x2 MIMO gain of 2, because of the antenna polarization, capacities up to 187 Mbps can be achieved.

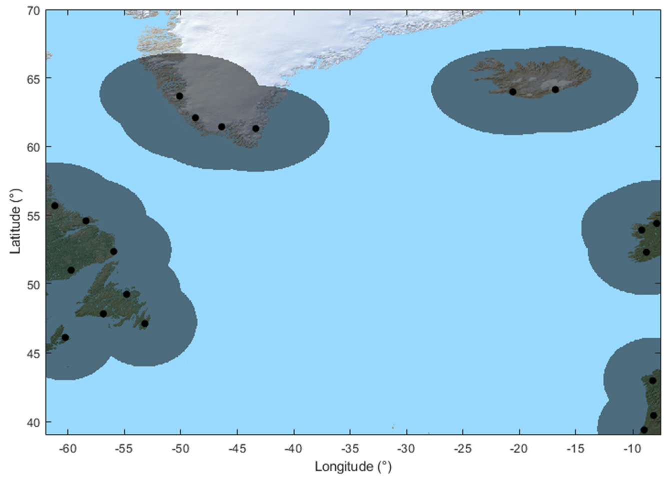

Fig. 3. Base station locations and their coverage. For Europe, the locations of BSs are the same as those of EAN. For North America, Greenland and Iceland, the locations of BSs are selected to cover a large area of the ocean with DA2GC.

3.2 Network Model

Our focus in this paper is on forming AANETs over regions such as oceans having no ground infrastructure to provide Internet connectivity in the sky. As a use case scenario, we focus on the North Atlantic Corridor due to the busy transoceanic routes for aircraft in this paper. This area is between -60° and -10° in longitude, and between 40° and 65° in latitude.

The ground DA2GC BSs are important elements to provide backhaul connectivity to the aircraft in AANETs. Hence, the locations of them are critical to maximize their coverage toward the ocean. For the European side, the locations of BSs used are those of the European Aviation Network [16]. For North America, Greenland, and Iceland, the BSs are assumed at locations near the sea to cover the greatest possible area in the ocean. More BSs can be deployed in case of congestion, however, we assume that the number of beams on a BS is always sufficient to serve the aircraft in its coverage area. The location of the BSs and the total covered area can be seen in Fig. 3. In combination with the assumed antenna gains, all DA2GC links can achieve the maximum possible data rate, which is 187 Mbps. For an aircraft to be connected in AANETs, it needs to have a data rate of at least β. The data rate threshold, β, is chosen per the capacity of DA2GC links, which are backhaul links for providing connectivity to AANETs. Hence, a selected β must be always smaller than 187 Mbps. However, the ratio of the data rate threshold and backhaul DA2GC link capacity directly affects the performance of the overall formation of the topology and allocation of rates. Higher backhaul link capacities via more advanced antenna technologies or carrier aggregation can be adapted in our network model.

4 Problem Formulation

As stated previously, we define the problem of combined topology formation and rate allocation for AANETs as a

TABLE 2
Optimization Parameters

Input	Explanation
$G(V,E)$	Graph G with all aircraft set V and all possible edges set E
D_n	Nodal degree of aircraft nodes
$c_{i,j}$	Capacity of link (i,j)
$\Phi(1/SINR)$	A function of SINR to calculate data rate
$P_{i,j}$	Received power at node j from node i
$I_{i,j}^{k,l}$	Binary parameter equals to one if link (i,j) receives interference from link (k,l)
β	Data rate threshold
M	A large value to satisfy big M constraints
Variables	**Explanation**
$\lambda_{s,d}$	Rate of each aircraft from source s to destination d
$z_{i,j}$	Binary topology variable for (i,j) link
$f_{i,j}^{s,d}$	Traffic flow on edge (i,j) from source s to destination d
$A_{\lambda_{s,d}}$	Binary variable equals to one if the rate of aircraft d satisfies β

MILP. The objective is to maximize the number of aircraft which have a higher data rate than a threshold β. We model the network as a graph $G=(V,E)$ which contains a set of vertices V and a set of all possible edges E. $V=V_A\cup V_B$, where V_A contains each aircraft d, and V_B contains each DA2GC BS s. The variable $\lambda_{s,d}\in\mathbb{R}_+$ defines the rate of each aircraft from the source s to the destination d with representing traffic flow assignments destined to each aircraft. Due to constraints in the nodal degree D_n for aircraft nodes, we need to select a sub-topology from the full topology. This decision is modeled by the binary topology variable $z_{i,j}\in\{0,1\}$, which is 1 if edge (i,j) is in the final sub-topology. The capacity of the links depends on the SINR as calculated in (5). Hence, $c_{i,j}\in\mathbb{R}_+$, is the capacity of each link (i,j), as a function of $1/SINR$, $\Phi(1/SINR)$. The function $\Phi(1/SINR)$ maps respective SINR levels to modulation schemes and the capacity of the link, which are shown in Table 1. The SINR depends on the received power $P_{i,j}$ at node j from node i and the received interference for the link (i,j) by link (k,l) as defined in Section 3. The binary parameter $I_{i,j}^{k,l}$ is one if link (i,j) receives interference from link (k,l), which captures the effect of antenna beamwidth on interference. The noise power is defined as N_0. The traffic flow on edge (i,j) from source s to destination d is denoted as $f_{i,j}^{s,d}\in\mathbb{R}_+$. The flow is measured in the same unit as the capacity. The objective of the optimization problem is to maximize the number of aircraft which exceed the defined data rate threshold β. It ensures that only aircraft which can receive a minimum data rate of β can connect. To formulate this problem, we define the binary variable $A_{\lambda_{s,d}}\in\{0,1\}$, which is one if the received capacity by an aircraft exceeds β. Consequently, the objective is to maximize the sum of $A_{\lambda_{s,d}}$ of all aircraft at one network snapshot, i.e., the total number of aircraft having at least data rate threshold β. With the given parameters and optimization variables outlined in Table 2, the MILP problem can be written as follows:

$$\text{maximize} \sum_{s\in V_B, d\in V_A} A_{\lambda_{s,d}} \tag{6}$$

subject to

$$\sum_{(k,j)\in E} f_{k,j}^{s,d} - \sum_{(j,k)\in E} f_{j,k}^{s,d} = \begin{cases} \lambda_{s,d}, & \text{if } k=s \\ -\lambda_{s,d}, & \text{if } k=d \\ 0, & \text{otherwise} \end{cases}$$
$$\forall s\in V_B,\quad \forall d\in V_A,\quad \forall k\in V_A \tag{7}$$

$$f_{i,j}^{s,d}\le M z_{i,j},\quad \forall\, s\in V_B,\quad \forall d\in V_A,\quad \forall (i,j)\in E \tag{8}$$

$$z_{i,j}=z_{j,i},\quad \forall (i,j)\in E \tag{9}$$

$$\sum_{i\in V_A} z_{i,n}=D_i\le D_n,\quad \forall n\in V_A \tag{10}$$

$$SINR_{i,j}=\frac{P_{i,j}}{N_0+\sum_{(k,l)\in E} I_{i,j}^{k,l}P_{k,j}z_{k,l}},\quad \forall (i,j)\in E \tag{11}$$

$$c_{i,j}=\Phi(1/SINR_{i,j}),\quad \forall (i,j)\in E \tag{12}$$

$$\sum_{s\in V_B,\ d\in V_A} f_{i,j}^{s,d}\le c_{i,j},\quad \forall (i,j)\in E \tag{13}$$

$$\lambda_{s,d}\ge A_{\lambda_{s,d}}\cdot\beta,\quad \forall s\in V_B,\quad \forall d\in V_A \tag{14}$$

$$\sum_{(d,j)\in E}\ \sum_{s\in V_B,\ d\in V_A} f_{d,j}^{s,d}\le A_{\lambda_{s,d}}\cdot M\quad \forall d\in V_A \tag{15}$$

The conservation of flows is ensured by constraint (7). Other than the source and destination nodes, the incoming flows to a node is equal to the outgoing flows from that node, shows the conservation of the flows. However, the generation of flows at the source node s, we have an overall flow of $\lambda_{s,d}$, while we have an overall consumed flow of $\lambda_{s,d}$ at the destination node d. Constraint (8) is a big M constraint ensuring that flows can only be placed on links in the sub-topology, with M being a sufficiently large parameter. All links in the sub-topology need to be symmetric, which is ensured by constraint (9). Constraint (10) implements the nodal degree limitation such that the number of connections of aircraft i, D_i must be smaller than nodal degree, D_n. Constraints (11) and (12) define the calculation of SINR and capacity, respectively. Constraint (13) restricts that the sum of all flows needs to be smaller than the capacity of the link. Constraint (14) forces $A_{\lambda_{s,d}}$ to 0 if an aircraft does not reach the threshold capacity. Additionally, the only aircraft which meet the data rate threshold β can forward capacity to others, which is stated in constraint (15).

The ultimate goal of maximizing the number of aircraft having a data rate higher than a threshold is formulated as an MILP problem in (6) with the constraints (7)–(15), which is non-convex due to the integer constraints. This formulation represents a multi-commodity flow problem. It means that each aircraft has its own flow demand resulting in multiple commodities between the source and aircraft. The multi-commodity flow problem is proven to be an NP-complete problem [40]. It is investigated for the low densities of aircraft over the North Atlantic Corridor in [1] since the formulated MILP is computationally intractable for a greater number of aircraft nodes. Due to this limitation and lack of a tractable mathematical structure, heuristic solutions are unavoidable [41]. Hence, we propose an efficient two-phase heuristic algorithm to form the topology and allocate rates. As an example scenario, we consider the North Atlantic Corridor with higher densities, i.e., having more than 60 aircraft.

TABLE 3
Notations Used in the Proposed Algorithm and Their Explanations

Notations	Explanation
$G(V, E, c)$	Graph G with all aircraft set V and all possible edges set E with their capacities c
a	Single node that combines all DA2GC BSs
t	Hypothetical destination node
R_{mcr}	Maximum concurrent rate
N_{mcr}	number of aircraft having maximum concurrent rate
N^{hops}	The vector holding the number of hops from each aircraft to the source
V_A	The set of aircraft
$e_{i,j}$	Edge between i and j
Γ_{unsat}	The set of unsaturated aircraft
Γ_{sat}	The set of saturated aircraft
R_{sat}	The set of rates of saturated aircraft
$f(i)$	Maximum flow between the hypothetical source node a and the hypothetical destination node t after allowing the capacity of aircraft i to infinity

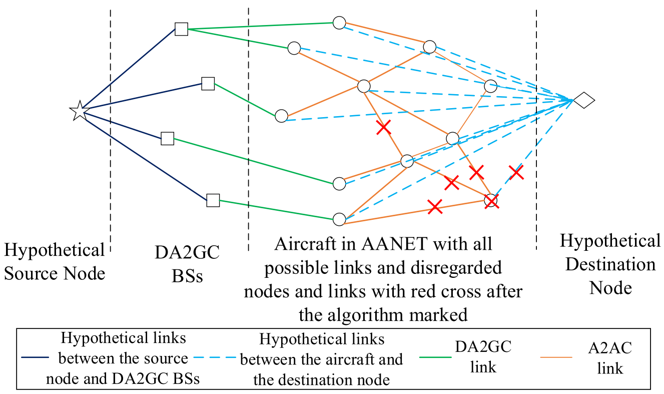

Fig. 4. Formed topology with hypothetical source and destination nodes.

5 Combined Topology Formation and Rate Allocation Algorithm

5.1 Overview of the Algorithm

For the initialization of the algorithm, all possible communication links are calculated to have a full topology. It includes the links among aircraft via A2AC and links between the BSs and aircraft via DA2GC as seen in Fig. 4. Note that Table 3 outlines notations for the explanation of the proposed algorithm. We assume that DA2GC BSs use beamforming, and there are always enough beams to serve aircraft connected to them. We combine all DA2GC BSs into a single node, a, for a simplified representation of ground backhauling for AANETs. Additionally, we assume that there is a hypothetical destination node, t, as seen in Fig. 4 for easier calculation of multi-commodity flows for each aircraft in the formed AANETs. The addition of the hypothetical nodes helps to present our heuristic algorithm in a simpler form. Furthermore, the links between aircraft and the hypothetical destination node are presented to model the flow of each aircraft. These links have the data rate of each aircraft. They are denoted by R_i for the aircraft i. The set of E contains all possible DA2GC and A2AC links for the initialization of the algorithm.

The set of aircraft is represented by V_A. Hence, the set of nodes in the graph G is $V = V_A \cup \{a, t\}$.

Algorithm 1. Topology Formation and Rate Allocation

Calculate available links based on distance /* *Formation of* $G(V, E)$ */
Calculate link capacities based on SINR values /* *Formation of matrix* c *to form* $G(V, E, c), c : E \rightarrow \mathbb{R}_+^2$ */
/* *Phase 1* */
Remove aircraft - RMA /* *Algorithm 2*/
Update link capacities based on SINR values /* *Update* $G(V, E, c)$*/
Remove links - RML /* *Algorithm 3*/
Update link capacities based on SINR values /* *Update* $G(V, E, c)$*/
Remove aircraft - RMA /* *Algorithm 2*/
/* *Phase 2* */
Rate allocation - RAA /* *Algorithm 4*/

Algorithm 2. Remove Aircraft Algorithm (RMA)

Input: The constructed complete graph $G(V, E, c)$, and data rate threshold β
Output: Updated $G(V, E, c)$
$R_{mcr} = MCRA(G, V, \emptyset, \emptyset)$ /* *Algorithm 5*
while $R_{mcr} < \beta$ **do**
  $N^{hops} =$ The vector holding the number of hops from each aircraft to the source
  $A = \{v | v \in V_A \text{ and } R_v = R_{mcr}\}$ /* *Calculate the vector of aircraft with the minimum data rate*/
  $A = \{v | v \in A \text{ and } N_v = max(N^{hops})\}$/* *Calculate the vector of aircraft with maximum number of hops* */
  $y = A(1)$ /* *The first element in vector A, which has the smallest index* */
  $G = G(V \backslash y, E \backslash \{e_{iy} | i \in V_A \backslash y\})$ /* *Remove y and its edges* */
  $R_{mcr} = MCRA(G, V, \emptyset, \emptyset)$ /* *Algorithm 5* */
end while

The proposed algorithm, Algorithm 1, finds a network sub-topology that includes as many aircraft as possible, all of which have data rates higher than a specified threshold. First, all the available links are determined, and the full topology graph, $G(V, E)$ is determined without any nodal degree or data rate constraints. Afterward, we calculate the capacities of the links as in (12) based on link SINRs on the full topology using (11) to obtain $G(V, E, c)$. c is a matrix for link capacities based on the calculated SINR of links in the topology. The next step for our algorithm is the removal of some aircraft in the current topology until the minimum data rate of the remaining aircraft is above the data rate threshold. Until this point, we have not considered nodal degree constraint, hence the following step is to remove some links to comply with the nodal degree requirement.

After removing aircraft links in the topology, the network might be degraded, which may result in some aircraft having a data rate lower than the data rate threshold. Therefore, the last step is to remove some aircraft again, to get the final topology. The reason for deleting aircraft at the beginning and end of the algorithm is to decrease the computation time. When an aircraft is removed, its associated links are also removed from the network as shown in Fig. 4 with red crosses, hence contributing to the link removal part. The link data rates are not calculated in each iteration of the algorithms regarding removing aircraft and links to increase computation speed. However, if they were recalculated at each step, an insignificant increase in the quality of the results is observed in our test cases. It has a greater impact on the cases with a high beamwidth, where the chance of a link interfering with others is higher. This explanation is a high-level description of Algorithm 1, and we provide more detail in the following subsections.

Algorithm 3. Remove Links (RML) Algorithm

Input: $G(V, E, c)$, maximum nodal degree D_n.
Output: Updated $G(V, E, c)$ with nodal degree constraint
$R_{mcr} = MCRA(G, V, \emptyset, \emptyset)$ /* *Algorithm 5* */
$N_{mcr} = count\{v | v \in V_A \text{ and } R_v = R_{mcr}\}$ /* *Find how many aircraft have the maximum concurrent rate* */
while $\Delta(G) > D_n$ **do**
  $B = \{v | v \in V_A \text{ and } deg(v) = \Delta(G)\}$ /* *B is the vector having the aircraft with the highest number of link connections* $\Delta(G)$ */
  $u = B(1)$ /* *The first element in vector B* */
  $A = \{v | v \in V_A \text{ and } c_{v,u} > 0\}$ /* *The vector of aircraft connected to aircraft z, which is the first aircraft in B* */
  $sort(A)$ based on number of connections
  $R_{temp} = 0,\ N_{temp} = 0,\ i = 1,\ Rates = \emptyset,\ Num = \emptyset$
  while $(R_{temp} \neq R_{mcr}\ OR\ N_{temp} \neq N_{mcr})\ AND\ i < length(A) + 1$ /* *loop stops when a subgraph* G_{temp} *which does not have a negative effect on the maximum concurrent rate is found, or until all the possible subgraphs are evaluated* */ **do**
    Copy G to G_{temp} and remove link between u=B(1) and $A(i)$
    $R_{temp} = MCRA(G_{temp}, V, \emptyset, \emptyset)$ /* *Determine maximum concurrent rate in new graph* G_{temp} */
    N_{temp} = number of aircraft which cannot increase their data rate further than R_{temp}
    Append R_{temp} and N_{temp} in $Rates$ and Num vectors, respectively
    Increment i
  end while
  if all possible subgraphs were evaluated **then**
    $P = \{y | y \in A \text{ and } R_y = max(Rates)\}$
    $P = \{y | y \in P \text{ and } N_y = min(Num)\}$
    $y = P(1)$ /* *Find all subgraphs whose maximum concurrent rate is the maximum from the ones calculated. From those, find the ones which have the minimum number of aircraft having this rate. If more than one are equal, choose the one with the smallest index* */
  else
    y = index of the last checked aircraft
  end if
  $G.e_{u,y} = 0$
  $R_{mcr} = MCRA(G, V, \emptyset, \emptyset)$
  $N_{min} = count\{v | v \in V_A \text{ and } R_v = R_{mcr}\}$
end while

5.2 Phase 1 - Topology Formation

The full topology includes all connections without any degree constraints. Hence, we remove some aircraft from the full topology in the first phase of the algorithm. The criteria for removing aircraft from the network are the minimum data rate and the number of hops to the source node, a according to Algorithm 2, namely, Remove Aircraft (RMA). First, we find the maximum concurrent rate, R_{mcr}, which is the minimum data rate that all aircraft have in the current topology, by Algorithm 5. More detailed information about the steps for finding R_{mcr} in Algorithm 5 are provided in Section 5.3. To give an overview of this algorithm, it iteratively estimates the rate of all aircraft according to a lower bound and an upper bound. These bounds are changed at each step until their difference is below a threshold to find the maximum concurrent data rate. It should be noted that the maximum concurrent data rate in the topology means the minimum data rate that can be achieved by aircraft in the network. Then, we create a vector A of aircraft having the maximum number of hops, $max(N^{hops})$, from the hypothetical source node a and having the minimum data rate found by Algorithm 5. We keep removing aircraft having the maximum number of hops from the hypothetical source node in the remaining topology until the maximum concurrent rate becomes greater than the threshold β. It generally results in keeping those aircraft having a smaller number of hops from DA2GC BSs than the removed aircraft.

Algorithm 4. Rate Allocation Algorithm (RAA)

Input: $G(V, E, c)$
Output: Final allocated data rates in graph G
Initialization: $\Gamma_{unsat} = V_A,\ \Gamma_{sat} = \emptyset,\ R_{sat} = \emptyset$
while $\Gamma_{unsat} \neq \emptyset$ **do**
  $R_{mcr} = MCRA(G,\ \Gamma_{unsat},\ \Gamma_{sat},\ R_{sat})$ /* *Algorithm 5* */
  $(\Gamma_{sat},\ \Gamma_{unsat},\ S) = FSAA(G,\ \Gamma_{unsat},\ \Gamma_{sat})$ /* *Algorithm 6* */
  $R = \{R_i = R_{mcr}\ \forall\ i \in S\}$ /* *Set R contains the data rates of the new saturated aircraft* */
  $R_{sat} = R_{sat} \cup R$
end while

The second step in Phase 1 is about deleting some links to comply with the nodal degree constraint. Algorithm 3, namely, Remove Links (RML) Algorithm, ensures that the nodal degree constraint, D_n, is satisfied. In general, removing links from the network will degrade the equal bandwidth allocation. In each iteration of this algorithm, the chosen link to remove is the one whose removal will have the least negative effect on the network. The effect of removing a link is measured by the calculated maximum concurrent rate, R_{mcr}, and the resulting number of aircraft having the maximum concurrent rate, N_{mcr}. The quality of the network decreases if R_{mcr} decreases or if N_{mcr} increases. Aircraft with a higher number of links are prioritized for the removal. Hence, the first link is removed from an aircraft u with the highest number of links. We denote the highest number of link connections in the current network as $\Delta(G)$. For each link between aircraft u and its connected aircraft set in A, the maximum concurrent rate after the removal of that link and the number of aircraft having the new maximum concurrent rate are calculated. If R_{mcr} or N_{mcr} remain the same by removing a link, this link is deleted. If there is no such link, then the one whose removal degrades the network the least is removed. The removed link is the link resulting in the maximum concurrent rate and the minimum number of aircraft having the new maximum concurrent rate. The procedure continues until all aircraft meet the nodal degree requirement.

Algorithm 5. Maximum Concurrent Rate Algorithm (MCRA)

Input: $G(V, E, c)$, Γ_{unsat}, Γ_{sat}, R_{sat}
Output: λ_0 as the maximum concurrent rate
Initialization:
$\lambda_u = max\{c_{x,y} |\ link\ (x, y) \in DA2GC\ links\})$
/ Initialize upper bound to maximum DA2GC capacity */*
$\lambda_l = \begin{cases} 0, & \text{if first iteration} \\ \text{previous max concurrent rate}, & \text{otherwise} \end{cases}$
while $\lambda_u - \lambda_l > \epsilon$ **do**
  $\lambda_0 = mean(\lambda_u,\ \lambda_l)$
  $R_i = \lambda_0, \forall i \in \Gamma_{unsat}$
  $R_j = R_{sat}, \forall j \in \Gamma_{sat}$
  $f = maxflow(a, t)$ */* find flow from hypothetical source a to hypothetical destination t */*
  if $f = \sum_{i=1}^{N_{air}} R_i$ **then**
    /* $N_{air} = |V_A|$ */
    $\lambda_l = \lambda_0$
  else
    $\lambda_u = \lambda_0$
  end if
end while
$\lambda_0 = (\lambda_u + \lambda_l)/2$

Removing the excess links in the topology to satisfy the nodal degree constraint may degrade link data rates. It may result in a data rate less than the threshold, β. Hence, we again run Algorithm 2 to ensure that the aircraft nodes in the final topology have a data rate of at least β.

5.3 Phase 2 - Rate Allocation

The second phase of the algorithm is the bandwidth allocation via Algorithm 4, i.e., Rate Allocation Algorithm (RAA). Outputs of this algorithm are the maximum data rates allocated to all aircraft in the final topology. This algorithm is a tailored version of the algorithm proposed by [42] with the utilization of Algorithm 5 instead of linear programming to decrease the computation time. Initially, none of the aircraft has a saturated data rate. Hence, the set of unsaturated aircraft is V_A, and the set of saturated aircraft is empty, i.e., $\emptyset$. We need to store the data rates of saturated aircraft in R_{sat}. It is initially $\emptyset$. Afterward, the aircraft, whose data rate cannot be increased further, are identified. These aircraft are saturated ones for the rest of the algorithm, while the others are unsaturated. For the next iterations, saturated aircraft keep the data rate previously calculated, and the maximum concurrent rate for the rest of the aircraft is computed again. The loop stops when every aircraft has received its allocated data rate.

Algorithm 5 bounds the maximum concurrent data rate λ between two values λ_l and λ_u. By setting ϵ sufficiently low, we can assume that $\lambda_0 \approx \lambda$. For our case, ϵ is 10^{-5}. Initially, the lower bound λ_l is set to 0, and the upper bound λ_u to $max(c_{x,y})$, where $c_{x,y}$ the capacity of the link between any DA2GC link (x, y). The exact value of λ lies between λ_l and λ_u. In each iteration, λ_0 is defined as $(\lambda_l + \lambda_u)/2$. Hence, the output of maximum concurrent rate algorithm (MCRA) in Algorithm 5 is an approximation of λ, i.e., λ_0, such that $|\lambda_0 - \lambda| < \epsilon$. The data rate of each unsaturated aircraft is set to λ_0, while the saturated aircraft keep the data rate calculated in previous iterations. Afterward, the maximum flow f_{max} from the hypothetical source to the hypothetical destination is calculated. If f_{max} is equal to the sum of all data rates, all aircraft can satisfy their demands, and therefore λ_0 can increase. λ_0 is now the new lower bound. If f_{max} is less than the sum of data rates, at least one aircraft cannot achieve data rate λ_0. Therefore, λ_0 is the new upper bound. In the next iteration, the difference between the two bounds is halved. The algorithm continues until $|\lambda_u - \lambda_l| < \epsilon$.

Algorithm 6 finds the new set of saturated aircraft with the allocated data rate calculated in Algorithm 5. For each unsaturated aircraft i, a temporary graph G_{temp} is created, where the data rate of i is set to ∞. Thus, aircraft i is allowed to increase its data rate if possible. The maximum flow from the hypothetical source to the hypothetical destination for each aircraft i, $f(i)$, is calculated. The aircraft i with $f(i) = min(f)$ are the ones whose data rate cannot be increased anymore. These aircraft are now considered saturated, and their data rate is the concurrent data rate calculated in the previous step.

Algorithm 6. Find Saturated Aircraft Algorithm (FSAA)

Input: $G(V, E, c)$, Γ_{unsat}, Γ_{sat}
Output: Set of saturated (Γ_{sat}) and unsaturated (Γ_{unsat}) aircraft, and set of aircraft with current maximum concurrent rate, S
Initialization: $f \in \mathbb{R}^{1xN_{air}}$, all its entries set to $+\infty$
for $i \in \Gamma_{unsat}$ **do**
  $G_{temp} = G$
  $R_i = \infty$ */* Capacity from aircraft i to destination t is set to be ∞ in G_{temp} */*
  $f(i) = maxflow(a, t)$ */* maximum flow between the hypothetical source node a and the hypothetical destination node t after allowing the capacity of aircraft i to infinity */*
end for
$S = \{v | v \in V \text{ and } f(v) = min(f)\}$
$\Gamma_{sat} = \Gamma_{sat} \cup S$
$\Gamma_{unsat} = \Gamma_{unsat} \backslash S$

6 Performance Study

6.1 Simulation Setup

To understand the impact of the different parameters, we analyze the connectivity for various cases. A total of 7 days from 09:30 on 3/11/2017 until 09:30 10/11/2017 were analyzed. The time interval between two consecutive time instances is 15 minutes. We consider snapshots of the network at these time instances. For each of those time instances, a snapshot of the air traffic data is taken, and then the resulting AANET is analyzed with different parameters. The investigated parameters are antenna steering angle θ, nodal degree D_n, beamwidth ψ, and data rate threshold β. Additionally, we evaluate a case where only a subset of all aircraft - in this case, only Star Alliance aircraft - forms the AANET. In each comparison, we include a reference scenario where $\theta = 90°$, $D_n = 3$, $\psi = 10°$ and $\beta = 75$ Mbps. These reference values for θ, D_n, ψ and β will not be changed in performance evaluation unless otherwise stated. It should be noted that the definition of the connectivity in performance evaluation is the percentage of aircraft in AANETs that have a data rate higher than β.

TABLE 4
Simulation Parameters

Parameter	Value
$G_{t,BS}$	14.5 dB
$G_{r,DA2GC}$	29.2 dB
$G_{t,A2AC}$	32.2 dB
$G_{r,A2AC}$	32.2 dB
P_T	20 dBW
f_{DA2GC}	5.8 GHz
f_{A2AC}	31 GHz
N	-132.1 dBW
K_{DA2GC} for en-route phase	15 dB
K_{DA2GC} for taking-off/landing phases	15 dB
K_{A2AC}	20 dB
h	10 km
$\max(d_{A2AC})$	700 km
$\max(d_{DA2GC})$	350 km
Reference : θ	90°
Reference : D_n	3
Reference : ψ	10°
Reference : β	75 Mbps

The altitude of the aircraft, h, is 10 km above the ground. Hence, the maximum distance that two aircraft can communicate is 700 km. The maximum communication distance between a DA2GC BS and an aircraft is 350 km. Table 4 summarizes simulation parameters we utilized in our performance study.

6.2 Effect of Rician Fading on the Connectivity

We first investigate the effect of channel gain due to Rician fading on the percentage of connectivity. Fig. 5 shows the cumulative distribution function (CDF) of connectivity relative percentage in AANETs. The connectivity relative difference is the absolute difference between connectivity percentages with PL only and with PL plus Rician fading divided by the connectivity percentage with PL only. The CDF in Fig. 5 is calculated based on all instances in the seven days of our interest.

Due to large K parameters for DA2GC and A2AC, the difference between the percentage of connectivity considering different channel models is zero with a probability of 0.42. Furthermore, the probability that the connectivity relative difference is smaller than 6% is almost 0.9. Due to large K values for DA2GC and A2AC channels, the differences in the connectivity percentages with and without fading are not significant. Hence, in our following performance analysis, we employ PL only to obtain a close approximation in the connectivity percentage, which also decreases computations to obtain the average behavior of the connectivity percentage over the fading channel. This approximation means that $|X_{i,j}|^2 = 1,\ \forall\ (i,j) \in E$ in (11).

6.3 Comparison Study

We study the performance comparison between the heuristic and optimal connectivity results in terms of connectivity percentage. It is a measure of the percentage of aircraft in the network having a data rate above β. Besides, we have defined an upper bound on the connectivity of aircraft, which is explained below.

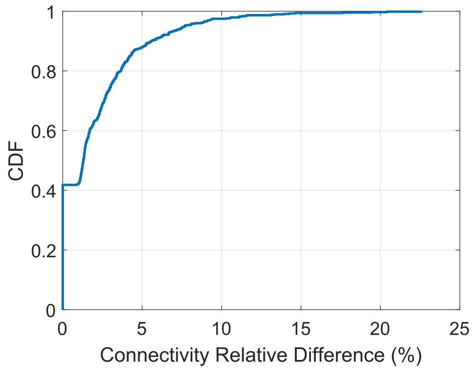

Fig. 5. Cumulative distribution function of connectivity relative difference between two cases where we consider path loss only and path loss with Rician fading.

An Upper Bound as the First Performance Benchmark: The upper bound on the number of aircraft achieving β is calculated by

$$\mu = \frac{C_{DA2GC}}{\beta}, \tag{16}$$

where C_{DA2GC} is the total backhaul capacity of all DA2GC links in the AANET. Hence, the upper bound on the percentage of connected aircraft in the network is calculated as $min(\mu/N_{air}, 1) \times 100$, where N_{air} is the number of aircraft in the network. $min(.,.)$ is used to avoid percentages higher than 100 when $\mu > N_{air}$. It should be noted that the upper bound computation ignores the nodal degree and topology constraints. The upper bound is utilized as a benchmark to measure the efficiency of our proposed heuristic algorithm.

Baseline algorithm Minimum Interference Spanning Tree [43] as the second performance benchmark: Our algorithm is compared with the Minimum Interference Spanning Tree Algorithm (MIST) presented at [43]. In this algorithm, the topology is created by choosing links causing the minimum interference. A minimum spanning tree is first created to ensure connectivity in AANETs from source node a to destination t. Afterwards, more links are added to the already connected nodes, until the connection limit is reached for all connected nodes. If the desired threshold is not reached, aircraft are removed from the topology until it is achieved.

A Lower Bound as The Third Performance Benchmark: This lower bound is obtained by considering the worst case scenario while forming AANETs. In step 2 of the Algorithm 1, link capacities are calculated for Algorithm 2, which removes aircraft that can not achieve maximum concurrent rate of β, which is the connectivity threshold. In the worst case scenario, the aircraft with DA2GC connectivity may not relay their data rate to other aircraft due to several reasons such as link distances and channel conditions. Hence, only the aircraft that are in the range of the DA2GC BSs (denoted as V_{DA2GC}) become connected, however, they are not able to relay their capacity to the other aircraft toward the ocean. It means that only the aircraft with DA2GC will exceed the data rate threshold. Hence, in the worst case scenario, Algorithm 5 returns the maximum concurrent rate as β with V_{DA2GC}, which can be written as follows:

$$\begin{aligned} &\beta = MCRA(G, \emptyset, V_{DA2GC}, \\ &R_{sat} = \{R_{sat}(i) \geq \beta, i \in \{1, \cdots, |V_{DA2GC}|\}\}). \end{aligned} \tag{17}$$

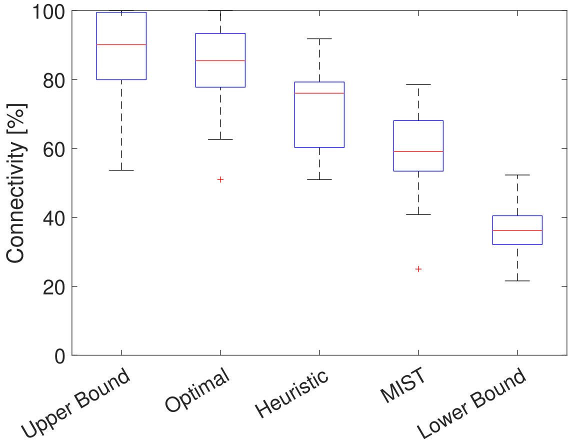

Fig. 6. Comparison of the connectivity percentages for the upper bound, the lower bound, the optimal from MILP formulation, our heuristic algorithm and MIST algorithm over all time instances in aircraft traffic data.

As the formed network is only limited to DA2GC links without A2AC relaying, the lower bound on the number of aircraft achieving β is given as

$$\Lambda = |V_{DA2GC}|. \tag{18}$$

A performance gap can be defined with the defined upper bound and lower bound on the number of connected aircraft. Our heuristic and optimal algorithm achieve to connect the number of aircraft, which is within the bound of $[\Lambda, \mu]$.

Fig. 6 shows the box plot of connectivity percentage of the upper bound, the optimal solution, our heuristic algorithm, MIST algorithm, and the lower bound for the percentage of the connectivity. To obtain box plots, we have utilized the aircraft traffic data to calculate the connectivity percentage of each method for all time instants. The optimal topology gives 7% worse connectivity than the upper bound connectivity in terms of the median connectivity. This result is expected, as the percentage for the upper bound is calculated such that all available DA2GC data rates are allocated to maximize the number of aircraft without considering nodal degree and interference constraints in the network. On the other hand, the solution from MILP considers the physical communication links between the aircraft and constraints (7)–(15). Hence, we observe such a difference between the upper bound and the optimal solution. Our heuristic performs approximately 8% worse than the optimal solution in terms of the median connectivity percentage. The results from the MIST algorithm are approximately 15% worse compared to our heuristic algorithm. The minimum connectivity percentage in AANETs is around 63% for the optimal solution whereas it is around 50% for the heuristic solutions. This drops to approximately 40% for the MIST algorithm. Furthermore, our heuristic performs almost 40% better than the lower bound in terms of the median connectivity. The lower bound is a special case considering the worst case possible in forming AANETs, where there are only DA2GC links. In the worst case, we can achieve maximum connectivity of 52% connectivity and minimum connectivity of 21%. Our heuristic algorithm can achieve a minimum connectivity of 51%, which means that at least the half of the aircraft are always connected. The results are derived from time instances with low aircraft densities to avoid high computational times for optimal topology calculations.

6.4 Implementation and Time Complexity of the Heuristic Algorithm

Our proposed algorithm uses the global information about the aircraft such as their route, speed, and locations over the North Atlantic Corridor. This information can be easily received by flight tracking systems such as FlightRadar. For the implementation of our solution, a central entity calculates the topology and allocated rates using our algorithm. The central entity can inform aircraft for their A2AC and DA2GC links and rates with simple message exchanges via already deployed satellite systems. These topology formations and rate allocation command messages can also be piggybacked to messages via satellites.

Time complexity of the proposed topology formation and rate allocation algorithm is dependent on the steps and corresponding sub-algorithms (i.e., Algorithms 2–6). The first two steps are the calculations of all physical links and capacities, which depend on the number of edges, i.e., $|E|$. The time complexity of these steps is $\mathcal{O}(|E|)$. In the worst case, it would be $\mathcal{O}(|V|^2)$, where $|V|^2$ is the maximum number of links in the graph G.

The first step of the first phase is to remove aircraft, which iterates over all nodes in AANETs and computes maximum concurrent rate. It depends on the number of aircraft, while the computation of the maximum concurrent rate is independent of the number of nodes. Hence, the time complexity of this step is $\mathcal{O}(|V|)$. The second step is to remove links, which requires searching links violating the nodal degree constraint. This search is over all edges. Hence, the time complexity is $\mathcal{O}(|E|)$. In the worst case, it can be regarded as $\mathcal{O}(|V|^2)$.

In the second phase, we compute the maximum concurrent rate for the unsaturated aircraft until there is no more unsaturated aircraft. In the iterations, we utilize "maxflow" from [44], which is shown to be an empirically efficient algorithm. The second phase needs to check the saturated nodes iteratively. Hence, its time complexity is $\mathcal{O}(|V|)$.

Among the steps outlined in Algorithm 1, the most time-consuming operations depend on $|V|^2$. Hence, the overall time complexity of the algorithm is $\mathcal{O}(|V|^2)$.

We also evaluate the required time that the algorithm needs to find a solution. The setup for this study uses a Matlab version of R2016b installed on a computer with Intel(R) Core(TM) i7-6700 CPU @ 3.40GHz and 32 GB RAM. The required time for a different number of aircraft is shown in Fig. 7. It shows a quadratic behavior with respect to the number of aircraft in the network, which is in line with our analysis of the time complexity of our algorithm. For our setup, it does not exceed 30 minutes, even for the highest aircraft densities.

Our proposed algorithm chooses a subtopology maximizing the number of aircraft with a data rate above the threshold. Hence, it starts with the full topology and deletes aircraft and links until the minimum rate in the subtopology is higher than the data rate threshold. For instance, if the data threshold is greater than the capacities of DA2GC links,

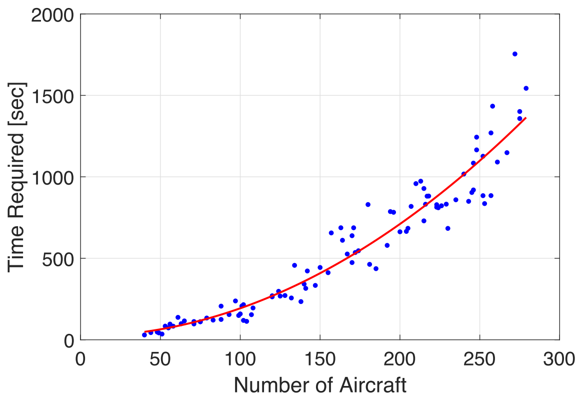

Fig. 7. Heuristic algorithm computation time.

our algorithm returns an empty topology. In such a case, even aircraft with DA2GC links are not connected. It is the worst-case scenario, but the algorithm converges to a trivial subtopology. If the data rate threshold is close to zero, our algorithm deletes the aircraft in the middle of the ocean without any connection to any BSs and deletes excess links to comply with the node constraints. The output of our algorithm will be a subtopology. Since our algorithm starts from full topology and iteratively decreases the size of the network, it will converge a subtopology that follows the constraints in the system settings.

6.5 Simulation Results

6.5.1 Maximum Steering Angle

The first parameter evaluated is the maximum antenna steering angle, θ. This variable affects the number of possible aircraft to which each aircraft can connect. Increasing the connectivity options by larger antenna steering angle improves the chances of finding links, which will provide better rate allocation among aircraft to achieve the data rate threshold. The effect of antenna steering angle can be seen in Fig. 8. The average connectivity for a 30° steering angle is 35% and increases to 42.1% for 90°. One main observation is that the connectivity over time follows the same pattern with the theoretical maximum. The effect of changing θ is visible clearly in Fig. 8. For the interval between 23:00 - 00:00 where the aircraft density is in its lowest level, the difference in the connectivity percentage between the AANETs with $\theta = 30°$ and $\theta = 90°$ becomes 10%.

Another important observation from Fig. 8 is that the lowest percentage of connected aircraft is attained while there is an increase in the number of aircraft in AANETs around 12:00 and around 04:00. The reason for such behavior around 12:00 UTC is that the first cluster of aircraft departing from Europe in the morning may not reach the other side, and most of them can not have a data rate higher than the threshold. Hence, we observe a decrease in the percentage of connected aircraft. The same situation occurs for the first cluster of aircraft from North America, which corresponds to the lowest percentage of the connected aircraft around 04:00 UTC. For the interval between 20:00 - 23:00 UTC, the number of aircraft over the North Atlantic Corridor decreases. Fewer aircraft can share the available capacity more efficiently to maximize the number of connected aircraft. Hence the percentage of connectivity increases. For

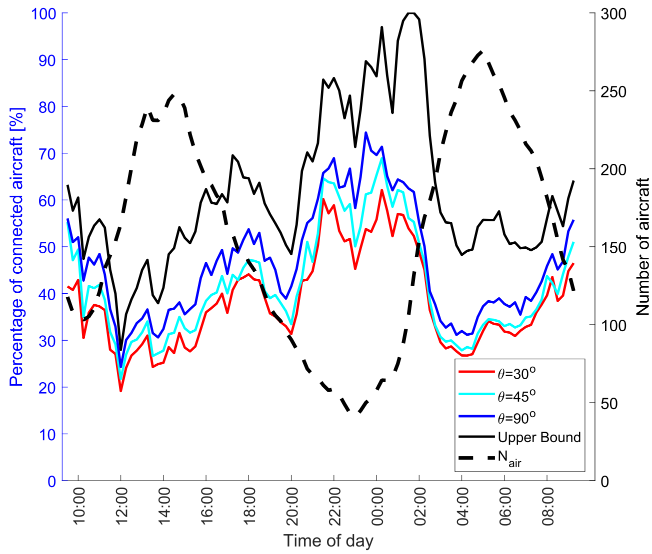

Fig. 8. Percentage of connected aircraft in different times of day in UTC for various maximum antenna steering angle values with upper bound and number of aircraft in the network.

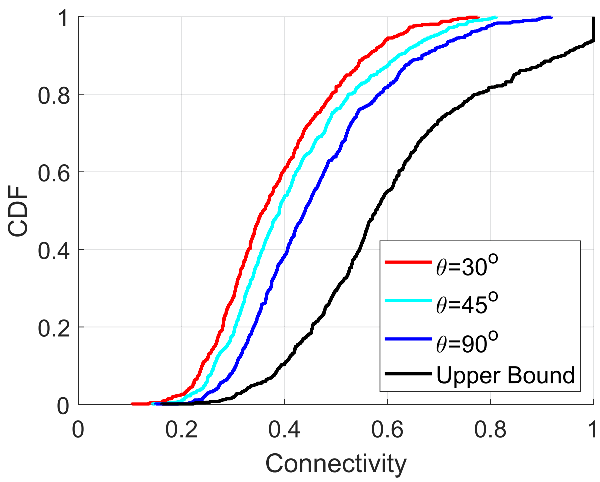

Fig. 9. Cumulative distribution function of connectivity for different maximum steering angle, θ, and their comparison with the upper bound.

the interval between 23:00 - 01:00 UTC, some aircraft from North America depart to provide backhaul capacity to the network since they are connected to DA2GC BS. Hence, an even better connectivity percentage is achieved.

We investigate the CDF of connectivity in AANETs for different maximum steering angles, θ, in Fig. 9. We also compare the CDFs associated with different θ with the upper bound. As seen in Fig. 9, the median connectivity for the upper bound is 0.57. On the other hand, it is 0.32, 0.36, 0.43 for $\theta = 30°$, $\theta = 45°$, and $\theta = 90°$, respectively. It results in a gap of 0.14 with the upper bound in terms of median connectivity when $\theta = 90°$. We observe these performance gaps since the upper bound calculations do not consider topology constraints. Since $\mu = C_{DA2GC}/\beta$ may get bigger than N_{air}, we observe a jump in the CDF of the upper bound when the connectivity equals 100%.

6.5.2 Nodal Degree

The maximum nodal degree depends on the number of antennas installed on each aircraft. A set of receiver/

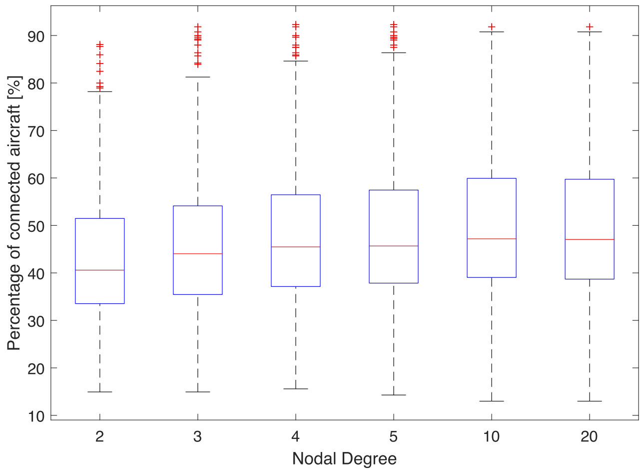

Fig. 10. Percentage of connected aircraft for different nodal degrees.

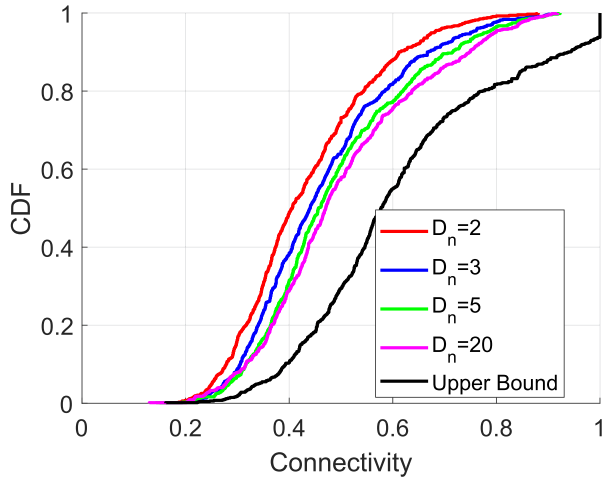

Fig. 11. Cumulative distribution function of connectivity for different nodal degrees, D_n, and their comparison with the upper bound.

transmitter antennas is required to establish a connection between two aircraft. Due to strict limitations on aircraft, it is important to evaluate the effect of the nodal degree to determine the number of installed antennas. As shown in Fig. 10, the nodal degree has a significant impact only when increasing from 2 antennas to 3, which results in median connectivity of 40.6% to 44%. Adding another 2 antennas only improves the results by 1.5%. Any further increase has a negligible effect on the results. Hence, increasing the nodal degree to more than 10 does not affect the connectivity percentage. One reason for this behavior is the increased interference due to the higher number of links, which decreases the capacity of links.

Fig. 11 shows a comparison among CDFs of the connectivity percentage in AANETs for different nodal degree, D_n, and the upper bound. As D_n increases, its effect on the connectivity percentage becomes negligible but approaches the upper bound. The median connectivity is 0.46 and 0.45 when $D_n = 20$ and $D_n = 5$, respectively. On the other hand, the median connectivity for the upper bound is 0.54, which is almost 20% better than the connectivity performance when $D_n = 20$.

6.5.3 Antenna Beamwidth

Interference is one of the most important metrics to determine the network topology. The beamwidth directly affects the interference in AANETs. Higher beamwidth causes more interference to the network, degrading the link quality. In Table 5, we study how the beamwidth affects the connectivity. Each column shows the percentage of aircraft exceeding the data rate threshold and cruising at a distance to the closest BS in the associated range of the first row. Since DA2GC links do not cause interference due to the capability of forming pencil beams, we can achieve 100% connectivity for aircraft up to 350 km from the closest BSs. For longer ranges though, the beamwidth has a significant impact on connectivity as in Table 5. For instance, among the aircraft cruising at a distance between 525 km and 700 km, more than 50% of those aircraft have a data rate higher than the threshold if beamwidth is zero degrees. In this case, A2AC links do not interfere with each other. As we increase the beamwidth to $40°$, we observe almost 40% drop

TABLE 5
Percentage of Connected Aircraft in Different Distances From the Closest BS for Various Beamwidths

Distance to the closest BS [km]	$\psi = 0°$	$\psi = 10°$	$\psi = 20°$	$\psi = 40°$
0 - 350	100%	100%	100%	100%
350 - 525	73.2%	67.6%	53.7%	23.7%
525 - 700	51.1%	43.7%	31.7%	14.3%
700 - 875	25.0%	21.1%	15.7%	8.0%
875 - 1050	10.9%	10.0%	8.2%	3.5%
1050 - 1225	5.9%	5.5%	3.7%	1.7%
1225 - 1400	2.8%	2.1%	1.1%	0.2%
1400 - 1575	1.8%	2.0%	0.9%	0.5%
1575 - 1700	0.4%	0.8%	0.0%	0.4%

in the connectivity due to greater interference. Hence, the beamwidth is one of the most important parameters affecting the connectivity over the North Atlantic Corridor.

For distances higher than 350 km to the closest BSs, having a beamwidth of $40°$ decreases the connectivity by 65.7% when compared to the reference case of $10°$. It should be noted that as mentioned in Section 5, that especially in the case of higher beamwidth, the algorithm would find better results if the link capacities were recalculated more frequently in the algorithm steps.

Fig. 12 shows a comparison among CDFs of the connectivity percentage in AANETs for different steering angles, ψ, and the upper bound. The impact of changing ψ on CDF of connectivity is significant as seen in Fig. 12. For instance, the median connectivity is 0.3 and 0.43 for $\psi = 40°$ and $\psi = 0°$, respectively. As the beamwidth becomes zero, the interference becomes almost zero. Hence, the performance of our algorithm approaches the upper bound closer due to having a more ideal system setup in terms of interference. However, the performance gap between the upper bound and our algorithm when $\psi = 0°$ is not zero since we are still obliged to the topology constraints.

6.5.4 Data Rate Threshold

The last parameter we analyzed is the required data rate, β, which is varied from 50 Mbps to 150 Mbps. As expected, a

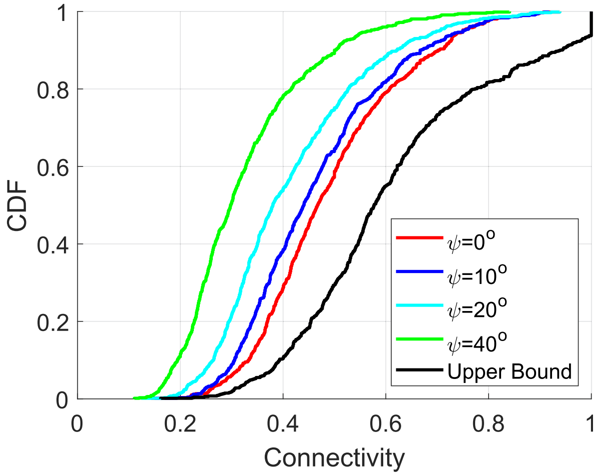

Fig. 12. Cumulative distribution function of connectivity for different beamwidth, ψ, and their comparison with the upper bound.

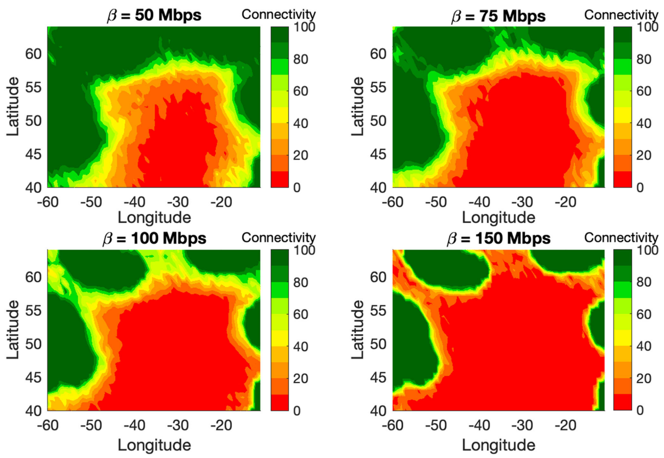

Fig. 13. Connectivity for different aircraft locations with various data rate thresholds.

lower threshold means a higher connectivity percentage. Increasing the threshold affects mostly the areas which are far from BSs. This is due to the fact that the algorithm prioritizes aircraft with a high number of hops from the BSs when removing aircraft. Aircraft which are connected to BSs with a small number of hops create more robust networks with lower delays and lower probability of lost packages due to fewer re-transmissions. As seen in Fig. 13, the areas close to the BSs have very high connectivity percentages. As we move towards the middle of the simulation area, where the distance to BSs increases, the connectivity drops rapidly. A big part of the simulation area has less than 10% connectivity. The areas with low connectivity expand as the threshold increases.

Fig. 14 shows a comparison among CDFs of the connectivity in AANETs with the upper bound for different data rate threshold, β. The parameter β has a direct impact on the evaluation of upper bound calculations due to (16). Hence, we can directly compare the performance of our algorithm and the upper bound for different β. When $\beta =$ 150 Mbps, the difference between the upper bound and our algorithm is the smallest. This is an expected result since the threshold is very high that only the aircraft close to the mainland can achieve. The median connectivity is 0.27 and

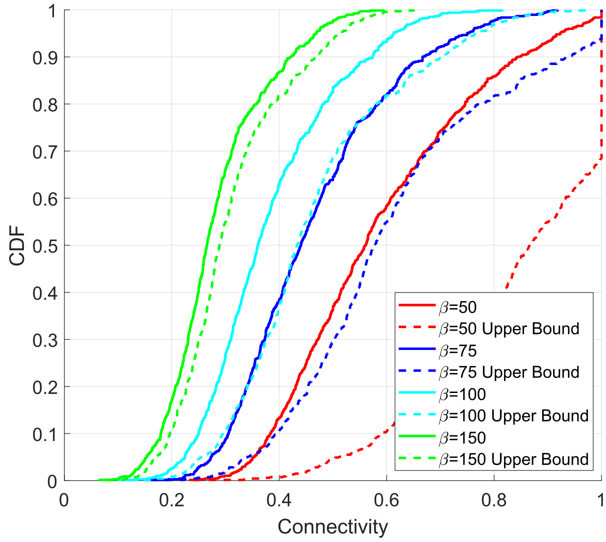

Fig. 14. Cumulative distribution function of connectivity for different data rate threshold, β, and their comparison with the upper bound.

0.28 for our algorithm and the upper bound, respectively, when $\beta = 150$. As β increases, it is more probable that most of the aircraft cannot achieve the data rate threshold. It results in a lower difference in the connectivity performance between our algorithm and the upper bound. On the other hand, the difference becomes larger between CDFs of our algorithm and the upper bound when the value of β decreases. Although lower β provides better connectivity, it is disadvantageous for our algorithm due to topology constraints. The upper bound calculation distributes the data rate of β according to the total DA2GC capacity, C_{DA2GC}. Hence, with lower β, we observe a higher difference in the percentage of connectivity between the upper bound and our algorithm.

The difference between the median connectivity of our algorithm and the upper bound is 0.01 when $\beta = 150$. The median connectivity of our algorithm for $\beta = 150$ is 0.27. Hence, the relative difference percentage is $0.01/0.27 \times 100$, which is less than 4%. The difference between the median connectivity of our algorithm and the upper bound is 0.30 when $\beta = 50$. The median connectivity of our algorithm for $\beta = 50$ is 0.57. Hence, the relative difference percentage is $0.30/0.57 \times 100$, which is more than 50%. We can conclude that the change in β provides more insight for the comparison of our algorithm and the upper bound due to the dependency of the upper bound on only β.

6.5.5 *Overall Evaluation of Network Parameters*

In [1], only the low-density cases are evaluated for optimal results. Their results show that the highest impact on the connectivity is the maximum steering angle, the lowest impact is antenna beamwidth. These outcomes are expected due to the low network density. A higher maximum steering angle helps find better connections in the neighborhood of aircraft to increase the connectivity in AANETs. Larger antenna beamwidth can not increase the interference substantially since there are not many neighbor aircraft. On the other hand, we study the performance of our algorithm for higher network densities in this paper. Results show that

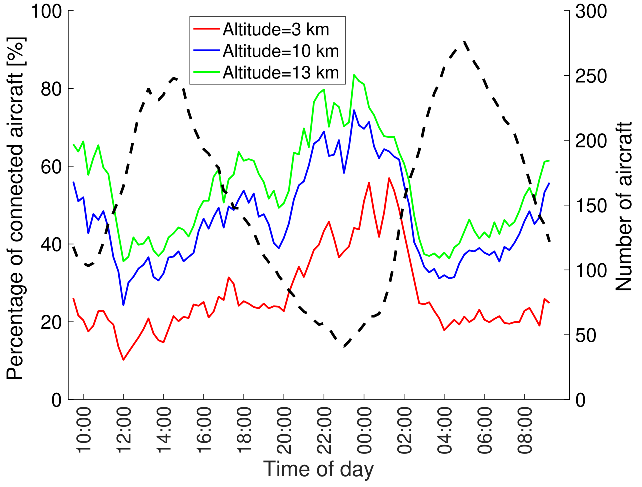

Fig. 15. Percentage of connected aircraft in different times of day in UTC for different altitudes.

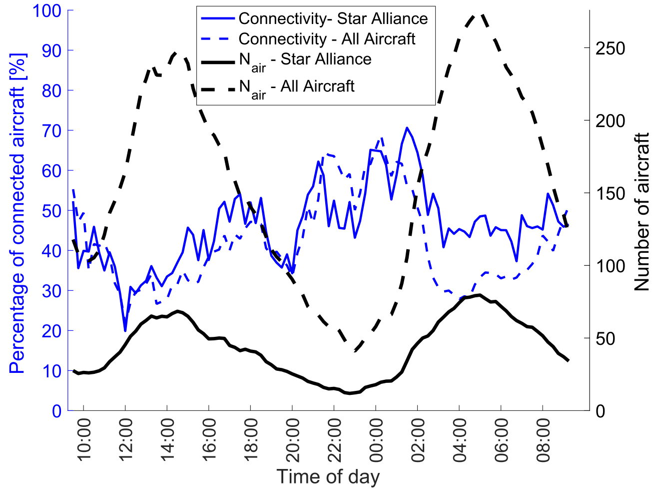

Fig. 16. Connectivity of the scenarios including Star Alliance aircraft and all aircraft in different times of the day.

nodal degree has the lowest impact when we look at the overall behavior for higher network densities. In higher network densities, three connections suffice to achieve the connectivity thresholds. Hence, the nodal degree becomes less important than the others. Furthermore, our algorithm has 25% lower performance than the upper bound on average in terms of connectivity for our reference scenario when we consider all network densities.

6.5.6 *Effect of Aircraft Altitude*

Another important parameter to investigate is the altitude of aircraft. It simply determines the maximum A2AC and DA2GC distances, which are related to the curvature of the Earth. As the altitude increases, the distance to the horizon increases, which is the cause of change in maximum A2AC and DA2GC link distances. If maximum A2AC link distance decreases, the number of neighbors that an aircraft can connect becomes fewer. Furthermore, a decrease in altitude of aircraft also decreases the number of aircraft that is directly connected to the DA2GC BSs, which limits the backhaul capacity towards the formed AANET over the North Atlantic Corridor. According to [5], for aircraft's altitude of 3, 10 and 13 km, the maximum A2AC link distance becomes approximately 400, 700 and 800 km, respectively. The maximum DA2GC distance is half of maximum A2AC link distance at respective altitudes. Fig. 15 shows that as we increase altitude in the network, we can have more aircraft that can be connected to the DA2GC BSs, which increases the backhaul capacity for the formed network. The connectivity data rate threshold is 75 Mbps. The main observation is that the deviation in the percentage of connected aircraft at 3 km of altitude do not change significantly between 10:00 and 18:00 despite the huge variation in the number of aircraft. At this altitude, we have very limited number of aircraft with DA2GC links, and they cannot also forward their data rate to their neighbors due to limited A2AC link distances. Hence, the percentage of connected aircraft at an altitude of 3 km is around 20% except between 21:00 and 03:00. On the other hand, when the altitude becomes 13 km, the minimum connectivity percentage is 20%.

6.5.7 *Consideration of a Subset of Aircraft Over the North Atlantic Corridor*

In a more preliminary scenario, only a subset of aircraft may form AANETs over the North Atlantic Corridor. As most airlines do not have enough aircraft to create a decent network over large oceanic areas, airline alliances such as the Star Alliance could be such as a subset of aircraft to form AANETs for providing connectivity overseas. This scenario is also analyzed to investigate if we can still have connectivity percentages similar to the scenario including all aircraft, and our results are summarized in Fig. 16. Two cases are considered; forming AANET with aircraft belonging to only Star Alliance and forming AANET with all aircraft over the North Atlantic Corridor. The two cases adopt the reference setup system parameters. We can see that in low densities the two scenarios have similar behavior. On the other hand, the Star Alliance network performs better in higher aircraft densities. This shows that even with the less number of aircraft, we can achieve the same performance in terms of the percentage of connected aircraft. Specifically, in time instances between 14:00 and 17:00 and between 02:00 and 08:00, the percentage of connectivity of Star Alliance aircraft is slightly better. This is due to the fact that even a small increase in the number of connected aircraft in these time instances has a greater impact on the percentage because of the significantly fewer number of aircraft in Star Alliance. Furthermore, due to the higher number of neighbors in all aircraft scenarios, there is more exposure to the interference from the neighbors which explains such behavior in those time instances.

7 CONCLUSION

In this article, we investigate topology formation and rate allocation in aeronautical ad hoc networks (AANETs) over the North Atlantic Corridor utilizing real aircraft traces. To this end, we formulate mixed-integer linear programming (MILP) to maximize the number of aircraft with a data rate exceeding a threshold subject to constraints on interference and antenna parameters. Since it represents a multi-commodity flow problem and is at least NP-complete, the optimal solution becomes computationally intractable for higher densities of AANETs. Hence, we propose a two-phase heuristic algorithm for topology formation and rate allocation to maximize the number of aircraft having a data rate higher than a threshold. Based on our performance studies, percentages of median connectivity for the MILP and the heuristic algorithm are comparable for low densities of AANETs. The connectivity varies between 40% and 70% depending on the density of the network for a data rate threshold of 75 Mbps. It shows that the overall DA2GC capacity is not sufficient to connect all aircraft with 75 Mbps. Hence, it is vital to increase DA2GC link capacity above 187 Mbps to achieve 100% connectivity with respect to a data rate threshold of 75 Mbps. Nevertheless, with a DA2GC link capacity of 187 Mbps, a guaranteed performance can be provided to 40% of the aircraft. The connectivity is also studied in terms of maximum antenna steering angle, nodal degree, antenna beamwidth, and data rate threshold and compared to an upper bound and a lower bound. In terms of average connectivity percentage, our proposed algorithm performs 40% better than the lower bound. Furthermore, the impact of nodal degree saturates after four. The other parameters have a significant impact due to their influence on the interference and they can achieve better performance in approaching the upper bound. We also investigate a scenario including only a subset of all aircraft, i.e., only aircraft belonging to Star Alliance. We show that this scenario has almost the same percentage of the connected aircraft compared to the scenario including all aircraft. With increasing node density, the difference in connectivity performance can reach up to 15% in favor of the Star Alliance scenario. Less node density is better for achieving higher connectivity percentages with the given threshold. Aircraft altitude also affects the connectivity percentage as it changes the network topology due to maximum distance for communication links. As the altitude increases, the distance to horizon increases, which in turn monotonically increases the number of neighbors that can be connected. As the altitude goes down from 13 km to 3 km, the maximum percentage of connected aircraft goes from 82% to 57%. As future work, we will investigate a design for service offerings such as minimum service guarantees for the topology formation and rate allocation problem Another future research direction is to capture the trajectory information in our model for topology reconfiguration in a dynamic scenario along with DA2GC BS deployment strategies.

Acknowledgments

An earlier version of this paper has been presented at IEEE ICC 2019 [1].

References

[1] S. Hofmann, V. Megas, M. Ozger, D. Schupke, F. H. P. Fitzek, and C. Cavdar, "Combined optimal topology formation and rate allocation for aircraft to aircraft communications," in *Proc. IEEE Int. Conf. Commun.*, 2019, pp. 1–6.

[2] J. G. Andrews et al., "What will 5G be?," *IEEE J. Sel. Areas Commun.*, vol. 32, no. 6, pp. 1065–1082, Jun. 2014.

[3] IATA, "IATA forecast predicts 8.2 billion air travelers in 2037," 2018. [Online]. Available: https://www.iata.org/pressroom/pr/Pages/2018–10-24-02.aspx

[4] NGMN Alliance, "5G White Paper," 2015. [Online]. Available: https://www.ngmn.org/wp-content/uploads/NGMN_5G_White_Paper_V1_0_01.pdf

[5] M. Vondra, M. Ozger, D. Schupke, and C. Cavdar, "Integration of satellite and aerial communications for heterogeneous flying vehicles," *IEEE Netw.*, vol. 32, no. 5, pp. 62–69, Sep./Oct. 2018.

[6] M. Vondra et al., "Performance study on seamless DA2GC for aircraft passengers toward 5G," *IEEE Commun. Mag.*, vol. 55, no. 11, pp. 194–201, Nov. 2017.

[7] E. Dinc, M. Vondra, and C. Cavdar, "Seamless gate-to-gate connectivity concept: Onboard LTE, Wi-Fi and LAA," in *Proc. IEEE 86th Veh. Technol. Conf.*, 2017, pp. 1–7.

[8] R. Wuerll, J. Robert, and A. Heuberger, "An overview of current and proposed communication standards for large deployment of unmanned aircraft systems," in *Proc. IEEE Aerosp. Conf.*, 2019, pp. 1–7.

[9] D. Minoli, *Innovations in Satellite Communications and Satellite Technology: The Industry Implications of DVB-S2X, High Throughput Satellites, Ultra HD, M2M, and IP*. Hoboken, NJ, USA: Wiley, 2015.

[10] M. Harris, "Tech giants race to build orbital internet [News]," *IEEE Spectr.*, vol. 55, no. 6, pp. 10–11, Jun. 2018.

[11] E. Dinc et al., "In-flight broadband connectivity: Architectures and business models for high capacity air-to-ground communications," *IEEE Commun. Mag.*, vol. 55, no. 9, pp. 142–149, Sep. 2017.

[12] Gogo Inc., ATG-4, "What is it, and how does it work," 2008. [Online]. Available: http://concourse.gogoair.com/gogo-atg-4-work/

[13] Gogo Inc., "Gogo 5G." [Online]. Available: https://business.gogoair.com/gogo-5g/

[14] Gogo Inc., "Gogo to launch 5G network in 2021," 2019. Accessed: Nov. 3, 2022. [Online]. Available: https://business.gogoair.com/news/2019/05/gogo-to-launch-5g-network-in-2021/

[15] SmartSky. Accessed: Nov. 3, 2022. [Online]. Available: https://www.smartskynetworks.com/

[16] European Aviation Network, "Partnering to bring high speed broadband to the skies of Europe." Accessed: Nov. 3, 2022. [Online]. Available: https://www.telekom.com/resource/blob/331302/c42355e291519c165e68d5b57f8519bf/dl-150924-euopean-aviation-netword-en-si-pdf-data.pdf

[17] Y. Zeng, R. Zhang, and T. J. Lim, "Wireless communications with unmanned aerial vehicles: Opportunities and challenges," *IEEE Commun. Mag.*, vol. 54, no. 5, pp. 36–42, May 2016.

[18] M. Sbeiti, N. Goddemeier, D. Behnke, and C. Wietfeld, "PASER: Secure and efficient routing approach for airborne mesh networks," *IEEE Trans. Wireless Commun.*, vol. 15, no. 3, pp. 1950–1964, Mar. 2016.

[19] I. Bekmezci, O. K. Sahingoz, and S. Temel, "Flying ad-hoc networks (FANETs): A survey," *Ad Hoc Netw.*, vol. 11, no. 3, pp. 1254–1270, 2013.

[20] B. Newton, J. Aikat, and K. Jeffay, "Analysis of topology algorithms for commercial airborne networks," in *Proc. IEEE 22nd Int. Conf. Netw. Protoc.*, 2014, pp. 368–373.

[21] S. Hofmann, A. E. Garcia, D. Schupke, H. E. Gonzalez, and F. H. P. Fitzek, "Connectivity in the air: Throughput analysis of air-to-ground systems," in *Proc. IEEE Int. Conf. Commun.*, 2019, pp. 1–6.

[22] D. Medina, F. Hoffmann, F. Rossetto, and C. Rokitansky, "Routing in the airborne internet," in *Proc. Integr. Commun. Navigation Surveill. Conf.*, 2010, pp. 1–10.

[23] M. Alzenad, M. Z. Shakir, H. Yanikomeroglu, and M.-S. Alouini, "FSO-Based vertical Backhaul/Fronthaul framework for 5G+ wireless networks," *IEEE Commun. Mag.*, vol. 56, no. 1, pp. 218–224, Jan. 2018.

[24] O. S. Oubbati, M. Atiquzzaman, P. Lorenz, M. H. Tareque, and M. S. Hossain, "Routing in flying ad hoc networks: Survey, constraints, and future challenge perspectives," *IEEE Access*, vol. 7, pp. 81 057–81 105, 2019.

[25] J. Zhang et al., "Aeronautical *AdHoc* networking for the internet-above-the-clouds," *Proc. IEEE*, vol. 107, no. 5, pp. 868–911, May 2019.

[26] FlightRadar24. Accessed: Jan. 20, 2021. [Online]. Available: https://www.flightradar24.com/

[27] E. Dinc, M. Vondra, and C. Cavdar, "Multi-user beamforming and ground station deployment for 5G direct air-to-ground communication," in *Proc. IEEE Glob. Commun. Conf.*, 2017, pp. 1–7.

[28] E. Dinc, M. Vondra, and C. Cavdar, "Total cost of ownership optimization for direct air-to-ground communication networks," *IEEE Trans. Veh. Technol.*, vol. 70, no. 10, pp. 10 157–10 172, Oct. 2021.

[29] M. Vondra, E. Dinc, and C. Cavdar, "Coordinated resource allocation scheme for 5G direct air-to-ground communication," in *Proc. Eur. Wireless Conf.*, 2018, pp. 1–7.

[30] K.-D. Buchter et al., "Drivers and elements of future airborne communication networks," in *Proc. Deutscher Luft- und Raumfahrtkongress*, 2012, pp. 1–10.

[31] C. Petersen, K. Fuger, and A. Timm-Giel, "Analytical model for aircraft-to-aircraft link probability over the north atlantic corridor," in *Proc. IEEE Veh. Technol. Conf.*, 2018, pp. 1–5.

[32] R. W. Kingsbury, "Mobile ad hoc networks for oceanic aircraft communications," Master's thesis, Dept. Aeronaut. Astronaut., MIT, Cambridge, MA, USA, 2009.

[33] D. Medina, F. Hoffmann, F. Rossetto, and C.-H. Rokitansky, "North atlantic inflight internet connectivity via airborne mesh networking," in *Proc. IEEE Veh. Technol. Conf.*, 2011, pp. 1–5.

[34] F. Hoffmann, D. Medina, and A. Wolisz, "Joint routing and scheduling in mobile aeronautical ad hoc networks," *IEEE Trans. Veh. Technol.*, vol. 62, no. 6, pp. 2700–2712, Jul. 2013.

[35] ETSI EN 303 316 V1.2.1, "Broadband direct airtoground communications; equipment operating in the 1 900 MHz to 1 920 MHz and 5 855 MHz to 5 875 MHz frequency bands; Beamforming antennas; harmonised standard for access to radio spectrum," Apr. 2018. [Online]. Available: https://www.etsi.org/deliver/etsi_en/303300_303399/303316/01.02.01_60/en_303316v010201p.pdf

[36] E. Haas, "Aeronautical channel modeling," *IEEE Trans. Veh. Technol.*, vol. 51, no. 2, pp. 254–264, Mar. 2002.

[37] U.S. Standard Atmosphere, "National oceanic atmosphere administration," Washington, DC, USA, 1976.

[38] S. O. Elbassiouny and A. S. Ibrahim, "Link level performance evaluation of higher order modulation in small cells," in *Proc. IEEE Int. Wireless Commun. Mobile Comput. Conf.*, 2014, pp. 850–855.

[39] J. Zyren, "Overview of the 3GPP long term evolution physical layer," Freescale Semiconductor Inc., 2007. [Online]. Available: https://www.nxp.com/docs/en/white-paper/3GPPEVOLUTIONWP.pdf

[40] S. Even, A. Itai, and A. Shamir, "On the complexity of time table and multi-commodity flow problems," in *Proc. 16th Annu. Symp. Found. Comput. Sci.*, 1975, pp. 184–193.

[41] T. ElBatt and A. Ephremides, "Joint scheduling and power control for wireless ad hoc networks," *IEEE Trans. Wireless Commun.*, vol. 3, no. 1, pp. 74–85, Jan. 2004.

[42] M. Allalouf and Y. Shavitt, "Centralized and distributed algorithms for routing and weighted max-min fair bandwidth allocation," *IEEE/ACM Trans. Netw.*, vol. 16, no. 5, pp. 1015–1024, Oct. 2008.

[43] V. Megas, "Aircraft to aircraft connectivity analysis," Master's thesis, Sch. Elect. Eng. Comput. Sci., KTH Royal Institute of Technology, Stockholm, Sweden, 2018.

[44] Y. Boykov and V. Kolmogorov, "An experimental comparison of min-cut/max-flow algorithms for energy minimization in vision," *IEEE Trans. Pattern Anal. Mach. Intell.*, vol. 26, no. 9, pp. 1124–1137, Sep. 2004.

Vasileios Megas received the diploma from the National Technical University of Athens, Greece, in 2016, and the MSc degree in wireless systems from the KTH Royal Institute of Technology, in 2018. Currently, he is working with Airbus in the area of Manned-Unmanned Teaming.

Sandra Hoppe received the MSc degree in electrical engineering from Technische Universität München, Germany in 2016 and the PhD degree from Technische Universitäat Dresden in 2021. In the same year she joined Airbus, Munich, Germany, where she was working on high capacity communication for aerial vehicles. In 2020, she joined Nokia Strategy & Technology in Munich, focusing on core network research and standardization.

Mustafa Ozger received the BSc degree in electrical and electronics engineering from Middle East Technical University, Ankara, Turkey, in 2011, and the MSc and PhD degrees in electrical and electronics engineering from Koc University, Istanbul, Turkey, in 2013 and 2017, respectively. Currently, he is a senior researcher with the KTH Royal Institute of Technology, Stockholm, Sweden and serves as a technical coordinator of EU Celtic Next 6G-SKY project. His research interests include 3D wireless networks and Internet of Things.

Dominic Schupke (Senior Member, IEEE) received Dr-Ing degree (summa cum laude) in electrical engineering and information technology from RWTH Aachen, Imperial College London, and TUM. He is a research leader in reliable communication networks, currently focusing on Wireless Communications at Airbus, Munich, Germany. He is also a lecturer in network planning with the Technical University of Munich (TUM). Prior to Airbus, he was with Nokia, Siemens, and TUM. He is author or coauthor of more than 150 journal and conference papers (Google Scholar h-index 32). His recent research addresses aerospace networks.

Cicek Cavdar is an associate professor with the School of EECS, KTH, Sweden. She has been leading the "Intelligent Network Systems" Research Group focusing on design and planning of intelligent network management and architectures, 3D network design and management considering non-terrestrial networks, and IoT connectivity. She coordinated the EU EIT Digital project "Seamless DA2GC in Europe," which has resulted in successful technology transfer cases to industry, and currently serves as the technical coordinator for EU AI4Green-AI for Green Networks, and 6G for Connected Sky projects. She served as symposium chair for IEEE ICC GCSN 2017.